J. Membrane Biol. 194, 97–108 (2003)
DOI: 10.1007/s00232-003-2029-5

The Journal of
Membrane
Biology

Identification of Caveolae-like Structures on the Surface of Intact Cells Using Scanning Force Microscopy

H. Lucius[1], **T. Friedrichson**[2], **T.V. Kurzchalia**[2], **G.R. Lewin**[1]
[1]Growth Factors and Regeneration Group, Department of Neuroscience, Max-Delbrück Institute for Molecular Medicine, Robert-Rössle-Str. 10, D-13122 Berlin
[2]Max Planck Institute for Molecular Cell Biology and Genetics, Dresden, Germany

Received: 22 October 2002/Revised: 10 April 2003

Abstract. Caveolae are small, functionally important membrane invaginations found on the surface of many different cell types. Using electron microscopy, caveolae can be unequivocally identified in cell membranes by virtue of their size and the presence of caveolin/VIP22 proteins in the caveolar coat. In this study we have applied for the first time scanning force microscopy (SFM), to visualize caveolae on the surface of living and fixed cells. By scanning the membranes of Chinese hamster ovary cells (CHO), using the tapping mode of the SFM in fluid, we could visualize small membrane pits on the cell membranes of living and fixed cells. Two populations of pits with mean diameters of around 100 nm and 200 nm were present. In addition, the location of many pits visualized with the SFM was coincident with membrane spots fluorescently labeled with a green fluorescent protein-caveolin-1 fusion protein. Scanning force microscopy on cells treated with methyl-β-cyclodextrin, an agent that sequesters cholesterol and disrupts caveolae, abolished pits with a measured diameter of 100 nm but left pits of around 200 nm diameter intact. Thus, the smallest membrane pits measured with the SFM in CHO cells were indeed very likely to be identical to caveolae. These experiments show for the first time that SFM can be used to visualize caveolae in intact cells.

Key words: Atomic force microscopy — Caveolae — GFP — Membrane pits — Methyl-β-cyclodextrin — Caveolin-1 — Cholesterol — Coated vesicles — CHO cells

Correspondence to: G.R. Lewin; email: glewin@mdc-berlin.de

Introduction

Techniques such as conventional or scanning electron microscopy have made it possible to investigate the fine structural organization of the cell surface. For some time it has been known that the membranes of many cells are rich in flask-like invaginations that have been named caveolae (Yamada, 1955; Anderson, 1998). These structures appear to be distinct from other types of membrane invaginations such as endocytotic vesicles or clathrin-coated vesicles by virtue of their size, lipid and protein composition (Anderson, 1998). Caveolae tend to be uniform in size with an opening diameter of between 50–70 nm when observed with the electron microscope (Rothberg et al., 1992; Maxfield & Mayor, 1997; Brown & London, 1998; Westermann, Leutbecher & Meyer, 1999). The caveolins, a family of integral membrane proteins, have been shown to be integral components of the caveolar coat (Rothberg et al., 1992; Kurzchalia et al., 1994). This caveolar coat in turn appears to be especially rich in cholesterol and glycosphingolipids (Fra et al., 1995; Murata et al., 1995). Caveolins are cholesterol-binding proteins and are capable of forming stable oligomers in the membrane (Monier et al., 1996).

Caveolae have been attributed various functions in cells, including membrane transport, regulation of intracellular calcium and signal transduction (Anderson, 1998). Several studies have shown that physiologically important signaling molecules might be clustered in or near the caveolae in intact cells (Okamoto et al., 1998; Kurzchalia & Parton, 1999). The hypothesis that caveolae also participate directly in the regulation of different signal-transduction events has recently been tested. Thus, a direct role for caveolin-1 and the caveolae system in Ras-mediated signal transduction in vivo was recently shown

(Roy et al., 1999; Scheel et al., 1999). In addition, analysis of a caveolin-1 knockout mouse has proven that this protein has an essential signal-transduction function in endothelial cells (Drab et al., 2001). The ever more compelling evidence that caveolae are physiologically important increases the need to develop new methods to study these organelles in intact cells.

The use of electron microscopy techniques is the only way to unambiguously identify and visualize caveolae in cell membranes. The very small size of the flask-like invaginations in the cell membrane (~50–70 nm diameter of the pore, 80–120 nm of the flask body; Westermann et al., 1999) has necessitated the use of the electron microscope. A complementary and less invasive approach has been to use immunofluorescence methods to visualize the caveolin protein that is predominantly localized in caveolae. Such studies reveal punctate fluorescence on the surface of cells that presumably reflects the presence of caveolae (Mayor et al., 1994). A third method has been to use preparative biochemical methods to isolate membrane fractions that are resistant to detergent treatment and are often described as caveolin-rich fractions. However, the identity of such caveolin-rich membrane fraction with morphologically identifiable caveolae is still controversial (Kurzchalia & Parton, 1999).

In the present study, we have evaluated a novel method, scanning force microscopy (SFM), for the identification and visualization of caveolae in intact cells. This method relies on the measurement of force interactions between a very fine tip and the cell membrane and under ideal circumstances can be used to measure the surface features of living cells to a resolution of 10 nm (Bustamante, Rivetti & Keller, 1997; Lesniewska et al., 1998). This technique has been used very successfully to study the architecture and dynamics of fusion pores in secretory cells such as pancreatic acinar cells (Schneider et al., 1997; Cho et al., 2002a), pituitary cells (Cho et al., 2002b) and endothelial cells (Goerge et al., 2002). However, there have been no studies published so far that have focused on the question of whether caveolae can be identified on the surface of cells with scanning force micrsocopy. We have used the SFM in tapping mode to image the surface of cultured Chinese hamster ovary (CHO) cells in culture. These cells are known to be rich in caveolae (Mayor et al., 1994; Lobie et al., 1999) and consequently topographical features on the cell surface indicative of caveolae might be observed using the SFM technique. Therefore, features imaged on the surface of both living and fixed CHO cells resembling pits were measured and quantified. In order to try and identify the molecular constituents of the surface pits, SFM was used on cells where a green fluorescent protein-tagged caveolin-1 fusion protein was simultaneously imaged on the cell surface. Additionally, we show that the smallest surface pits observed in our experiments disappeared after depletion of membrane cholesterol, indicating that they are identical to caveolae. This is the first evidence that caveolae can be observed in living cells with scanning force microscopy and introduces a new methodology for the study of these membrane structures.

Materials and Methods

Cells and Preparation

CHO cells were seeded on glass coverslips treated with Cell Tak (Beckton-Dickenson) and incubated in DMEM medium with 10% FCS and the following supplements: 2 mM Glutamine; 0.34 mM (45 μg/ml) Asparagin, 0.15 mM (17 μg/ml) Proline; and 100 units/ml Penicillin, 100 μg/ml Streptomycin. After the cells had attached, flattened and developed filopodia (about 20–24 h later), they were fixed with 3% PFA for 15 min at 20°C followed by a 3×5 min wash in PBS and stored at 4°C until measurements with the SFM were made. In parallel experiments, living cells were then scanned immediately with the SFM at room temperature.

Cloning and Transfection

Caveolin-1 (VIP-21) bearing EGFP at its N-terminus was produced as follows: GSVIPGS (Monier et al., 1996) was digested with *Bam*HI and *Kpn*I. To obtain pEGFVIP, the fragment was cloned into pEGFP-C1 (Clontech) cut with *Bgl*II and *Kpn*I. For inducible expression, the Ecdysone-inducible expression system (Invitrogen) was utilized. PEGFVIP was digested with nhe and *Bcl*I and subcloned into pIND (Invitrogen) cut with *Nhe*I and *Bam*HI-producing pINDEGFPVIP.

CHO EcR cells were maintained in Ham's F12 medium supplemented with 10% FC, 2 mM L-glutamine, antibiotics and 250 μg/ml Zeocin. After transfection with pINDEGFPVIP, using the calcium phosphate precipitation method, permanently transfected clones were selected by adding 0.5 mg/ml G418 to the growth medium. Expression of EGFPVIP was induced by addition of 5 μg/ml muristerone A.

One clone of the CHO cell line (CHO ECR pINDEGFPVIP) was seeded as above in the same medium containing in addition 0.36 mM (250 μg/ml) Geneticin G418 (SIGMA) and 0.22 mM (250 μg/ml) Zeocin (Invitrogen). Ten hours after plating, between 1 μM and 5 μM Muristerone A (SIGMA) solution in medium was applied to switch on GFP expression. Between 40 to 60 hrs later, when the cells showed fluorescence, protein synthesis was stopped with the addition of 35 μM (0.1 mg/ml) Cycloheximide (SIGMA) for 2 hrs. This ensured that most fluorescent caveolin protein was present on the membrane and not in the trans-Golgi. Cells were fixed as described above before the SFM experiments were carried out.

Cholesterol Depletion Experiments

CHO cells were seeded on a 60 mm plastic Petri dish (Peske) and divided with a DakoPen line (DAKO) into halves; 20–24 hrs after seeding, the cells were washed twice with serum-free medium. One part was treated with 10 mM methyl-β-cyclodextrin (SIGMA) in serum-free medium for 1 h at 37°C, 5% CO_2, followed by two washes in PBS at 37°C, and finally fixed as described above. Each

half (control and experimental) was treated identically except for the cyclodextrin treatment.

Scanning Force (SFM) and Optical Microscopy

SFM measurements were carried out using NanoScope IIIa (Digital Instruments, Fremont, CA) combined with an optical microscope Zeiss Axiovert 135, equipped with a CCD-Camera QuantiCam (PHASE, Lübeck, Germany).

Fluorescence microscopy was performed using a Leica Microscope DM RBE (Leitz, Wetzlar, Germany) equipped with a CCD camera (Hamamatsu C4742-95, Japan), image analysis was carried out using Openlab vers. 1.7.7 package (Improvision, Coventry, UK). Using the deconvolution software of the Open lab suite, images collected were routinely subjected to a digital confocal algorithm before alignment with the SFM images (*see* below).

The SFM measurements of membrane topography were carried out exclusively using the tapping mode of the instrument. Our experience of imaging fixed cells indicated that the results achieved in contact mode were never as good as those in tapping mode. The same was observed when imaging living cells. In all the experiments described here, V-shaped oxide-sharpened silicon-nitride cantilevers of type DNP-S, 0.38 N/m (Digital Instruments) were used. The optimal scanning speed ranged from 0.6 to 1.6 Hz for scan fields less than 16 μm^2. The amplitude decay of tip oscillation was set to about 20–30 nm for fixed and 5–15 nm for living cells when applying an oscillation voltage of 0.4–1.6 Vrms. Quadrates of the membrane of living cells were scanned twice (up-down or vice versa). Thus, only objects recognizable in both images were accepted. Each selected cell was scanned at high resolution at several different positions between the edge of the cell and the nucleus.

Data Processing

SFM images were processed using the NanoScope III software (vers. 4.23r3, 1997). Data was subjected to 1-D flattening, partially 2-D in scan direction and 3×3 Median filtering, to suppress streaks in the scan direction. The pit measurement was mostly carried out on zoomed subimages. For all membrane invaginations, which we will refer to in this paper as "pits", we measured the size (diameter or area-equivalent diameter if not perfectly spherical) and depth. This analysis was carried out using the section-analysis suite of the software. The diameter of a pit was measured as the horizontal distance at half-value level of the pit's profile, and the depth as it's full depletion. Although depth information was collected, we did not further analyze this data.

The alignment of SFM images and fluorescence-labeled caveolin-1 spots was done using two different approaches. In the first case, a montage of high-resolution scans (6–8 μm) was assembled into a low-resolution scan of the same cell region (16–20 μm). Cell contours as well as the edges of the cell were used as landmarks for alignment. For digital confocal microscopy, a series of fluorescent images was collected at 0.1-μm intervals, using a computer-controlled focus drive. This stack of images at different focal planes through the cell was then subjected to digital confocal analysis. From the fluorescence image stack, the membrane part that had been scanned using SFM was cut out and re-scaled. From each of the 0.1-μm layers of the stack, the "upper" fluorescence spots were transferred to an additional "membrane spot" layer. This layer represents the projection of the spatial fluorescence-spot distribution within or close to the cell-membrane surface. Spots present over several (more than three) layers were not included, as they were presumed to originate from structures within the cytoplasm (e.g., Golgi apparatus). This membrane fluorescence-spot layer was aligned with the SFM images, using additional information from the phase contrast picture. Finally, the fluorescence-spot layer (together with the contour) was overlaid onto the SFM image montage and rotated and shifted by eye until its contour fitted the SFM image contour, using the Corel Draw 7.0 software.

In later experiments, fluorescence images were captured simultaneously with the SFM scans of the same membrane area. This was achieved by using an oil objective to capture an image of the fluorescent membrane spots at a focal plane coincident with the pre-engaged SFM tip on the surface of the cell. This tip was then used to scan a quadrant of membrane that could then be aligned with a cropped area of the fluorescence image.

Statistical analysis was carried out using the STATISTICA software package (version. 5.1, J, StatSoft Inc. Tusla, OK). As data in the experiments (fixed—living and treated—control) were statistically independent samples with clearly non-normal distributions (Figs. 4 and 6), we applied the non-parametric Mann–Whitney *U* and the Kolmogorov-Smirnov-two-sample tests.

Furthermore, we fitted the size distributions of pits with a user-defined nonlinear estimation to ask whether the populations of measured pits consisted of two or more normally distributed subpopulations. First, the original data was fitted with a model described by a closed function. Deciding on the basis of Q–Q- and P–P-plots (StatSoft, 1997), the log-normal model proved to be the best fit for both populations. This model served as reference in estimating the histograms by a combination of user-defined functions, taking the squared residuals as losses. An approximation by two (or three) normal distribution functions was found to be the most appropriate model (*see* Results).

Results

The CHO cells were grown on the surface of glass covers slips (or in later experiments, on plastic). The cover slips were placed on the stage of an inverted microscope equipped with the scanning force microscope. Cells with a flattened morphology were imaged from above in fluid with the scanning force probe and the same cell could always be simultaneously observed under phase-contrast optics during scanning. It was important to be able to observe the cells during imaging, as the forces exerted on the cell by the tip could sometimes be enough to damage or move poorly adhered cells from the surface of the cover slip. Only data obtained from cells that remained intact during the course of the imaging experiment were included in this study.

Size Distribution of Membrane Pits in Living and Fixed Cells

Randomly selected regions of the membrane were chosen and scanned at high and low resolution in fluid. High-resolution scans of the surface of cells (scan areas from 4 by 4 μm to 2 by 2 μm) revealed small circular pits or indentations of various sizes in the membrane. These pits were observed on the surface of both fixed and living CHO cells (Fig. 1). In order to study whether some of these structures might have a size and spatial arrangement similar to caveolae, we took a more quantitative approach. This

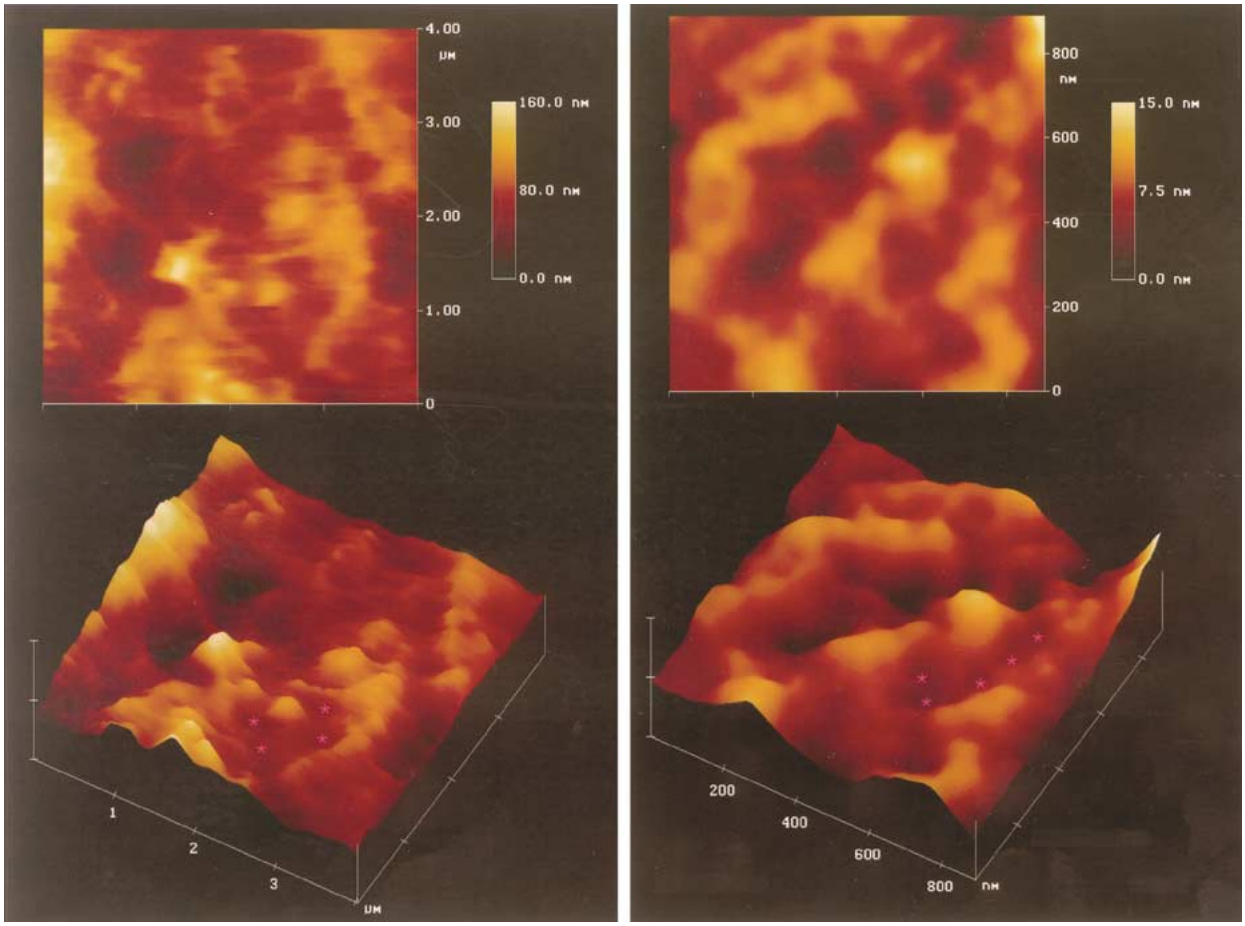

Fig. 1. Examples of membrane topography from the surface of CHO cells acquired in tapping mode with the SFM. The same region of the cell membrane is shown in 2-D (*top*) as well as in a 3-D projection (*bottom*). The images shown on the left were acquired from an intact living CHO cell, whereas that on the right is taken from a lightly fixed cell. In both 3-D images, one cluster of pits is indicated with an asterisk placed over each member of the cluster. Note that in each image more pits are present than indicated by asterisks. The resolution of the topographic images was, as shown here, typically much better with lightly fixed cells.

Table 1. Summary of data obtained from CHO cells

	Experiment I		Experiment II	
	Fixed	Living	β-Cyclodextrin-treated cells	Untreated Cells
Preparations	3	3	3	3
Cells	12	14	13	10
Pits total	595	331	552	463
Pits in groups	491	272	530	452

consisted of measuring the exact size of a large number of pits at different cellular locations on many different cells, both living and fixed. For each experiment, at least 330 pits were measured on the surface of at least 10 different cells (*see* Table 1). The characteristics of the pits measured on different cells were very consistent. Qualitatively, the membranes of the scanned cells exhibited a variable number of pits that tended to be clustered together on the membrane in groups of 2 to 10 (Fig. 1). This clustering of the surface pits is very reminiscent of the observation that caveolae also appear to be orientated in elongated clusters on the surface of MDCK cells (Rothberg et al., 1992).

Pits were randomly selected from the processed images and their dimensions measured with the aid of the section-analysis tool of the digital instrument software. Using this tool, the diameter of the pit and the depth were measured. Pit diameter did not appear to vary according to the location of the pit on the cell

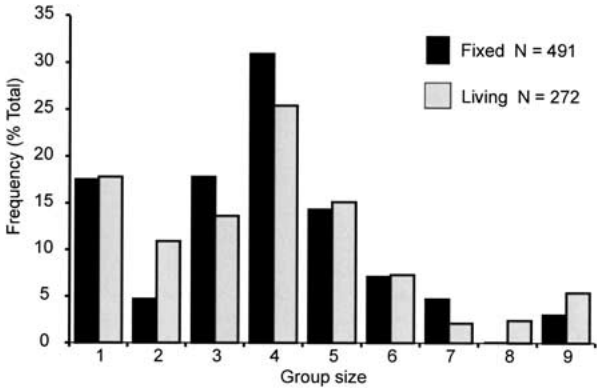

Fig. 2. Frequency of pit group size. The relative frequency with which pits were observed to occur as singles or in groups of 2–10 is plotted. The definition of a group can be found in the methods. It can be seen that the tendency for most pits to congregate in groups of 3–5 is the same in living and fixed preparations.

surface, for example, near the edge of the cell or near the centrally located nucleus. Pits tended to be more numerous at the leading edge of the cells. Pits were divided, using subjective criteria, into clusters consisting of 2–10 pits. The criteria for assigning pits to groups was that the pit was within a maximum of 1 μm of a member of the group and that the total distance was less than twice that between any two members of the apparent group. Using these criteria, the most common group size was between 3–5 pits. Interestingly, this clustering of pits was essentially the same when the pits were measured in fixed or in living preparations (Fig. 2). We next asked if pits of a uniform size tended to have a characteristic group size. This did not appear to be the case, as the size distribution of pit diameter was the same for all groups consisting of between 2 and 10 pits (*data not shown*). Single pits not associated with nearby clusters of pits proved the exception, as the size distribution of these pits was very broad and unimodal with a mean diameter of 350 nm. In contrast, the size distribution of pits observed in clusters was clearly multi-modal (*see* below). We took this observation to indicate that these single pits could at least in part be random topographical features of the surface, exhibiting features similar to pits or that they represent another type of surface organelle. We have excluded the measurements of single pits from the statistical analysis described below. These single pits made up only a very small part of the total data set (*see* Table 1) and when they were included in the analysis, the major results described below were not altered (*data not shown*).

The size distribution of measured pit diameter on the surface of lightly fixed and living cells is plotted in Figure 3. It is clear that both size distributions look very similar and a statistical analysis indicated that the distributions were not significantly different

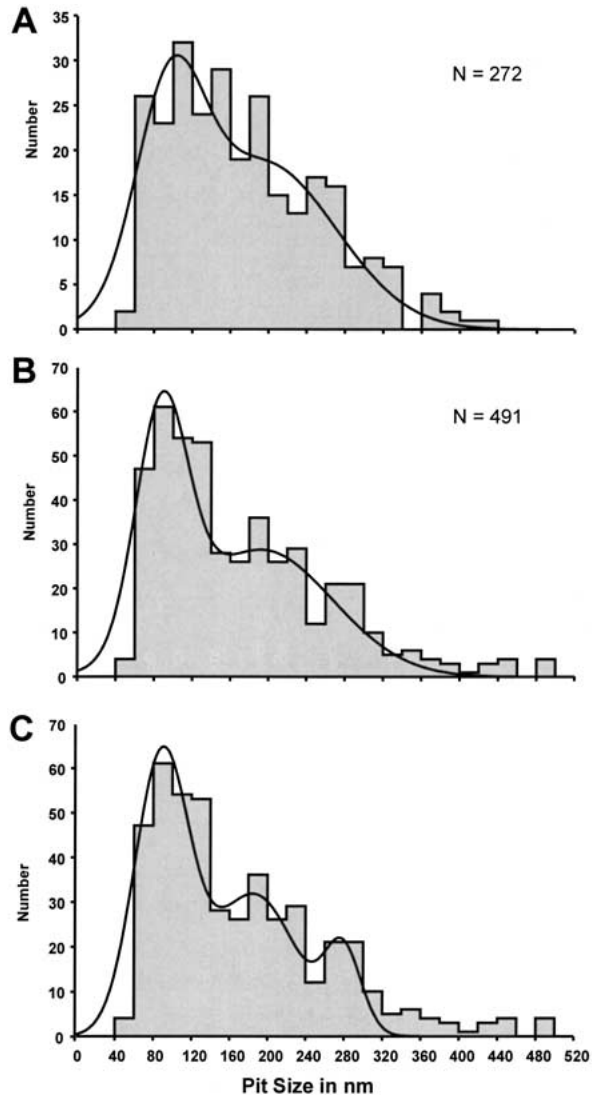

Fig. 3. Size-frequency histograms of pits measured with the SFM. (*A*) Size distribution of pits measured in living CHO cells. (*B* and *C*) Corresponding data plotted for CHO cell imaged after light fixation. In *A* and *B* the raw data has been fitted to two normal distributions plotted on top of the raw data. It can be seen that the two normal distributions with approximately the same means for living and fixed cells described the data well. In *A*, data were taken from living cells, the means are 96 and 195 nm for the two fitted distributions. In *B*, data were taken from fixed cells; the means of the two fitted normal distributions was 88 and 186 nm. In *C*, the same data from fixed cells was fitted to three normal distributions, which had means of 89, 186 and 279 nm.

(Kolmogorov-Smirnov test, $p > 0.10$, Mann–Whitney U test, $p = 0.52$). Thus it is likely that the pits measured in both living and fixed cells are essentially the same. For both living and fixed cells it is clear that the pit diameter size distribution is not a normal one. Instead, there appear to be at least two and possibly three distinct peaks in the diameter distribution. In other words, the entire distribution may be explained by two or three kinds of pits with

diameters that are themselves normally distributed. A statistical analysis of the residuals (sum of squares of deviation) obtained with a closed-function log-normal fit of the raw data and a user-defined function assuming two or more normal distributions was then carried out. The data from fixed and living cells was used in the statistical analysis, although individual peaks appeared to be better resolved in the fixed cells (Figure 3). A closed log-normal function described the data well with a residual of 1063; however, a much better fit was obtained using a user-defined function that assumed two underlying normal distributions (residual 669). The fit was only slightly better when an underlying distribution of three normals was assumed (residual 571). When we used the same general equation to fit the data with two normal distributions, it was interesting to note that the mean diameter estimates from living cells, 96 nm and 195 nm, was very similar to that from fixed cells, 88 nm and 193 nm. The use of three normal distributions for the fixed-cell data did not significantly alter the diameter estimation of the pits falling into the small and middle population (smallest 89 nm, middle 186 nm and largest 279 nm). This analysis also clearly indicated that the proportion of pits that were large, was very small (<10%) compared to the small and medium-sized pits. If the two main populations of pits are biologically distinct entities, the smallest pits appear to make up approximately 60% of the total with the medium-sized pits, diameter 186–195 nm, the remaining 40%.

Colocalization of GFP-Caveolin Fusion Proteins with Pits Imaged with Scanning Probe Microscopy

In order to ask whether a subset of membrane pits observed with scanning-probe microscopy were indeed caveolae, we used a CHO cell line stably expressing an inducible caveolin-1 GFP fusion protein. Between 40 to 60 hours after addition of the steroid hormone muristerone, GFP-labeled caveolin-1 protein can be observed with the fluorescent microscope in the Golgi and in small spots in the plasma membrane. This technique has the key advantage that caveolae are fluorescently labeled without the need to use antibodies, which would involve permeabilization and thereby loss of membrane integrity. We took the spots on the plasma membrane to be identical to endogenous caveolae, where the GFP-caveolin-1 protein is localized. We wished to ask whether these fluorescent spots could be mapped to pits in the membrane imaged with scanning-probe microscopy on the same cell. The spatial resolution of the fluorescent microscope in conjunction with digital confocal microscopy is, however, much worse than the resolution obtained with scanning-probe microscopy. We thus decided to ask if the *pattern* of fluorescent caveolin spots could be mapped to the *pattern* of pits obtained with the SFM image from the same cells. In theory, the coordinates of every fluorescence spot cannot be accurately mapped to individual pits, as the resolution of the two techniques is not compatible. However, if the two-dimensional pattern of fluorescent spots can be aligned approximately with the SFM-imaged pits this would indicate that molecularly tagged caveolae are indeed imaged as pits in the SFM image. An overlay from such an experiment is shown in Fig. 4. In this experiment, several consecutive image layers are captured and the fluorescence image deconvolved (digital confocal) using the Openlab image analysis software. Because the surface features of the cell are not flat in each image, the uppermost fluorescent spots (optical section 0.1 μm) represent surface spots on only part of the cell. The spots that were judged to be on the surface were therefore gathered together in one image that was aligned with the composite SFM scan of the same cell. The edge of the cell, outlined from the phase contrast image, was used to help in aligning the SFM image and the fluorescent image (details in Materials and Methods). Because an absolutely accurate alignment is impossible, it was difficult to make any conclusions about the size of the pits that might be colocalized with the fluorescent spots. However, in all three cells examined it was possible to make an alignment similar to that shown in Fig. 4. What was immediately noticeable after detailed examination of the alignment was that the majority of the fluorescent spots (shown in green) were found near or on top of single pits or clusters of pits. Very few of the spots were found in topographical locations lacking pits.

In later experiments, this approach was further refined so that the SFM image and the fluorescence image could be more directly compared. First, an image of fluorescent spots was captured using a high-power oil immersion objective. The SFM tip was prepositioned onto the membrane surface so that scanning could commence after an image of the tip was

Fig. 4. Colocalization of GFP-labeled caveolin with membrane topography. In *A*, two deconvolved fluorescent image layers (*6* and *7*) are shown from the SFM-scanned cell. The fluorescent spots that appeared in no more than three consecutive 0.1-μm thick layers from the surface of the cell were merged together for alignment with the SFM images. In *B*, the composite fluorescent image has been placed over and aligned with the SFM topographical image. The bottom half of the latter SFM image is a montage of several smaller high resolution scans of the membrane. It can be seen that the green caveolin-positive spots tend to be localized with pits in the SFM image. Examples are circled with a yellow dotted line.

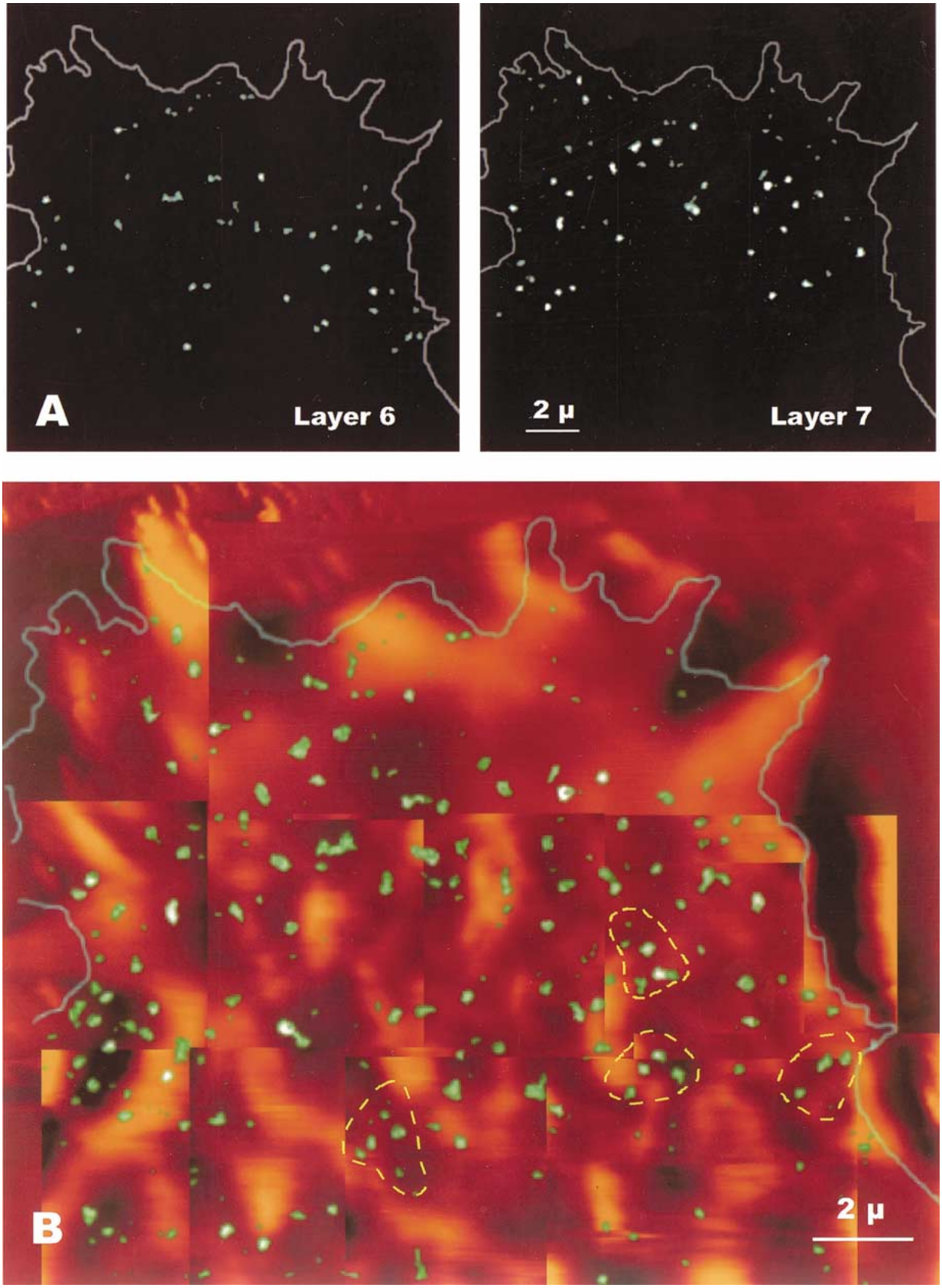
A
Layer 6
2 µ
Layer 7
B
2 µ

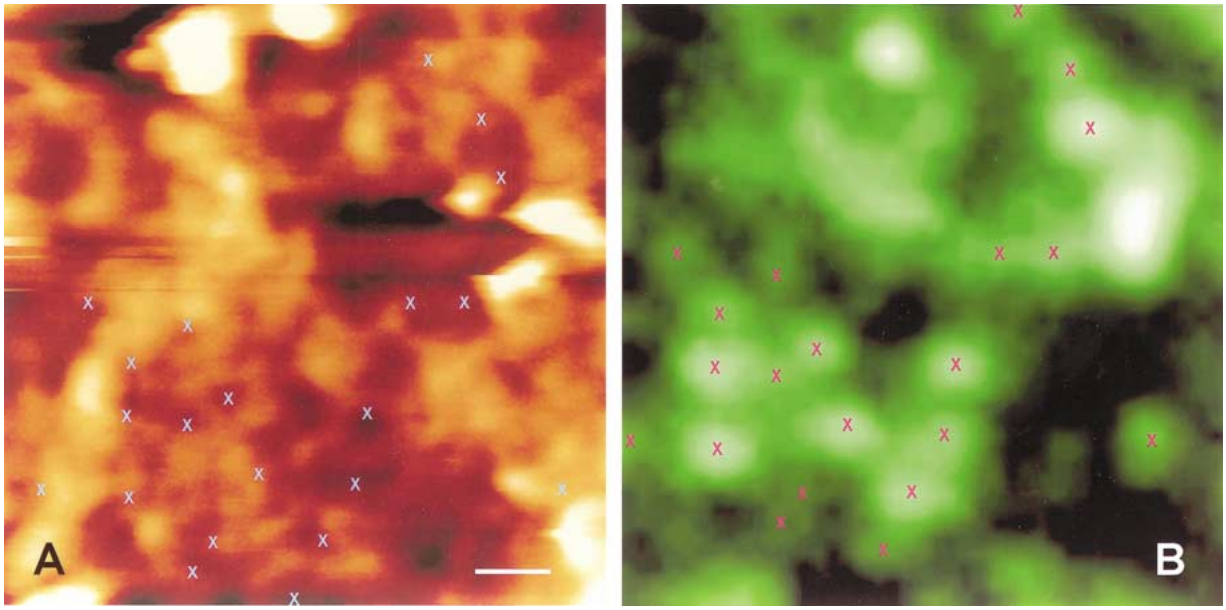

Fig. 5. Colocalization of GFP labeled caveolin-1 spots with SFM scans, using the same microscope. In *A*, the SFM image obtained after capturing the fluoresenct image shown in *B*. Crosses indicate green fluoresent spots that appeared to be on the surface; note that these crosses often correspond to recognizable pits in the SFM image. Scale bar is 250 nm.

focused and captured using epifluoresence illumination (tip engaged but scan field set to zero). The fluorescent image could then be rescaled to correspond to the SFM scan size and the two images then directly superimposed. Lateral displacement of the two images probably occurred due to slippage of the specimen during the SFM scan; we estimated this error to be in the order of 0.5 μm. This procedure worked well in some cases but was often fraught with difficulties, as the quality of the fluorescence images was often good but the SFM scan was not successful or vice versa. An example of such a scan is shown in Fig. 5, in this particular case, a very good correlation was found between surface fluorescence spots and pits in the SFM scan. It often appeared that intense and large regions of fluorescence did not correlate so well with surface pits and this may be because most of the caveolin-GFP was in this case in intracellular compartments. In summary, although good correlation between the localization of caveolin-1-GFP and surface pits was observed, this technique still did not allow us to unequivocally identify the surface features so that we can designate pits as caveolae.

Effects of Cholesterol Depletion on Membrane Pits

The bimodal size distribution of pit diameter found on CHO cell membranes suggested that two functionally distinct membrane organelles might underlie this distribution. It was striking that our data indicated that a population of small membrane pits with a mean diameter of around 90 nm might exist in the CHO cell membrane. This is very similar to the diameter of caveolae estimated from electron microscopy experiments. It is known that treatment of cells with agents that deplete cholesterol from the membrane disrupt these organelles (Rothberg et al., 1990; 1992; Schnitzer et al., 1994). Treatment of cells with methyl-β-cyclodextrin is an efficient way of sequestering cholesterol from the plasma membrane (Ohtani et al., 1989; Kilsdonk et al., 1995; Keller & Simons, 1998) and is effective in disrupting caveolae (Rodal et al., 1999). In order to determine whether one of the two populations of pits we describe was dependent on membrane cholesterol, we treated one set of cells with methyl-β-cyclodextrin and measured cell surface features in the same way as described above in parallel with untreated cells from the same culture. As a control we also treated the CHO cell line expressing inducible GFP-caveolin-1 with methyl-β-cyclodextrin after induction of GFP-caveolin-1. Fluoresence microscopy experiments showed that membrane-associated GFP-caveolin-1 was efficiently disrupted one hour after treatment with methyl-β-cyclodextrin (*data not shown*).

A summary of the data collected in this second set of SFM imaging experiments is shown in Table 1. The gross morphology of cells after treatment for one hour with the methyl-β-cyclodextrin was unchanged compared to untreated cells. Again random areas of the membrane were scanned at high resolution and diameter distributions of the measured pits constructed. In these experiments, the mean diameter of the control population was not different from that measured in the first set of experiments, although in the experi-

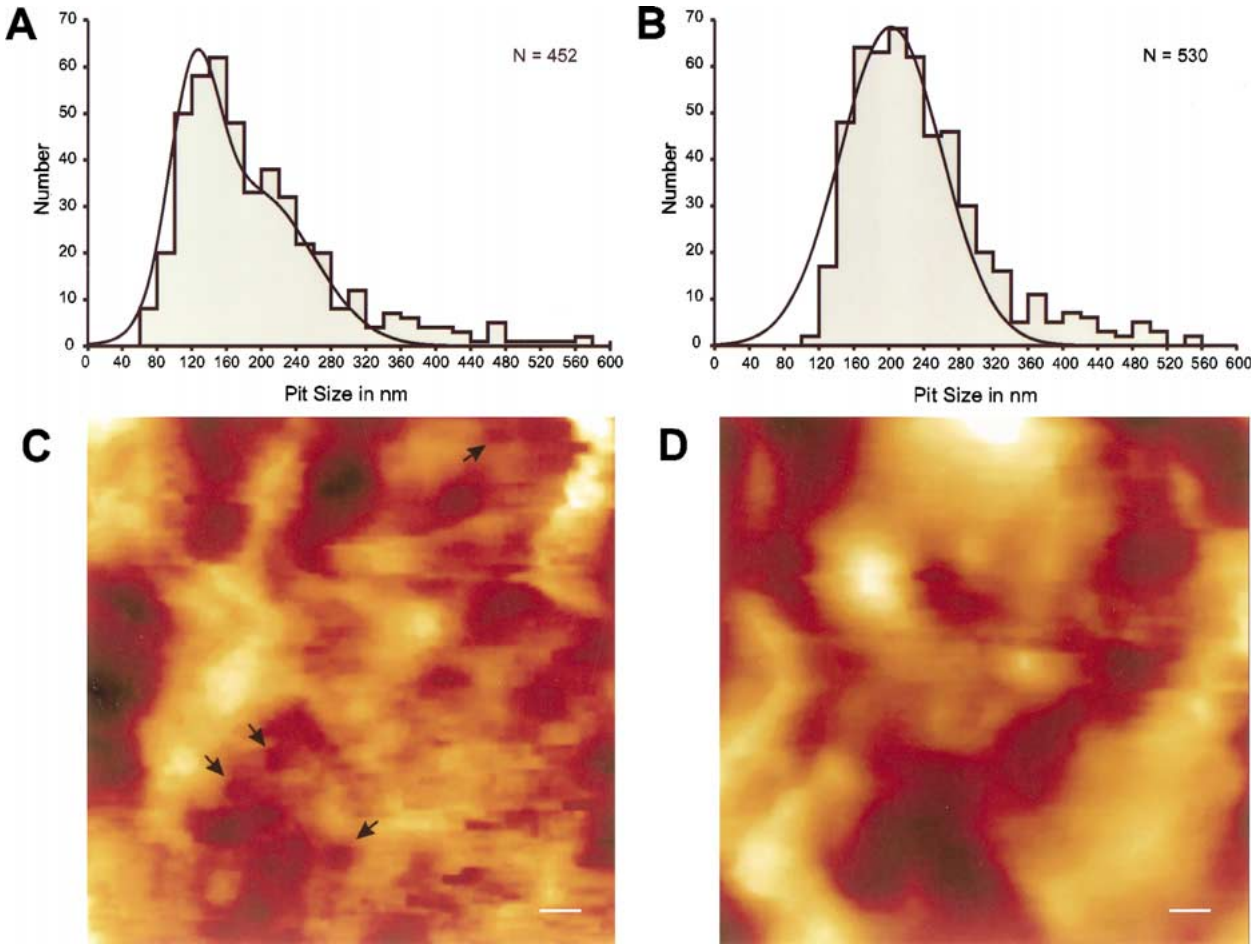

Fig. 6. Size distribution of pits after treatment with methyl-β-cyclodextrin. In a second series of experiments, two sets of lightly fixed cells were imaged in parallel. One group served as control (*A*) and the second group (*B*) was treated with methyl-β-cyclodextrin, an agent that depletes cholesterol from the plasma membrane. In each case, the size distribution of the imaged pits is shown and the data has in each case been fitted with one or two normal distributions, as described in Results. The control group was best described by the presence of two distinct groups of pits with a mean diameter of 121 and 195 nm, similar to that found in the first series of experiments. However, after cholesterol depletion the data was best described by the presence of only one group of pits with a mean diameter of 203 nm. An example of a high-resolution scan of the membrane in control (*C*) and methyl-β-cyclodextrin-treated cells (*D*) is also shown. Note that in the latter case, the membrane lacks very small pits that may correspond to cavaeloe. Scale bar is 200 nm.

mental series pits larger than 600 nm were excluded. Thus the data could again be fitted with two normal distributions, indicating two distinct sets of pits with a mean diameter of 122 and 195 nm. In the parallel series of cells treated with methyl-β-cyclodextrin, pits were also observed and randomly selected areas from the membrane were scanned in the same way as for the control population. In this case, the diameter distribution looked markedly different from the control cells (Kolmogorov-Smirnov test, $p < 0.001$), with the peak of the distribution apparently shifted to larger diameters (Fig. 6). Fitting the data by a user-defined function of one or more underlying normal distributions revealed the best fit was achieved with just one normal distribution with its peak at 203 nm. It appeared, therefore, that the smaller pits with a mean diameter of 90–122 nm were almost completely missing from the cell surface. Examples of pits measured on control cells and cells treated with methyl-β-cyclodextrin are shown in Fig. 6. It is clear that treated cells lack a population of membrane pits of small diameter. The pits that remained on the membrane after cholesterol depletion also appeared to be present in clusters like in the control cells. However, there was a definite tendency that the group size had decreased compared to control (Fig. 7). This finding might indicate that normally the larger membrane pits are clustered into smaller groups.

Discussion

In this study we have applied scanning force microscopy (SFM) to the study of caveolae in intact cells.

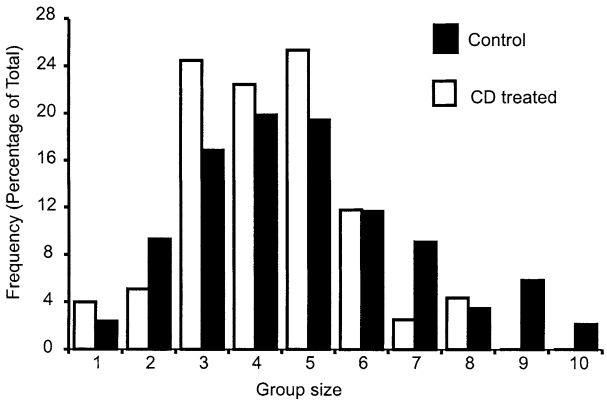

Fig. 7. Mean group size of pits after methyl-β-cyclodextrin treatment. Note that after cholestrol treatment, the largest group size to which pits could be assigned was apparently decreased.

Since it is known that caveolae are abundant on the surface of CHO cells in culture, we have asked whether one can image these structures with SFM. In order to unambiguously identify membrane indentations or pits as caveolae we have combined SFM with the use of cells expressing green fluorescent protein-tagged caveolin-1 and the experimental manipulation of surface caveolae, using cholesterol depletion with methyl-β-cyclodextrin. On the surface of both living and lightly fixed cells, we observed what appeared to be pits of various sizes, often clustered together on the membrane. Interestingly, these pits were not uniformly distributed in size but were best described by the presence of at least two populations of pits with diameters of around 100 and 200 nm, respectively. The mean diameter of the small diameter pits imaged in these experiments was about 30% larger than published estimates of the pore diameter of caveolae made from ultrastructural studies (Rothberg et al., 1992; Westermann et al., 1999). Thus the initial data suggested that a substantial number of the smallest pits imaged with the SFM might be identical to caveolae. Due to the nature of the SFM imaging method, it is more likely that the measured pit size would be an overestimate. This is because abrupt changes in surface topography tend to be rounded out during imaging, as in tapping mode, the tip cannot exactly follow very abrupt changes in surface contour (Bustamante et al., 1997). It is interesting that our data indicate that essentially the same two populations of pits were present in both living and fixed cells despite the fact that the membrane is easier to image in the second case, due to its increased stiffness.

In order to verify that the topographical features observed with the SFM corresponded to functionally identified caveolae we combined the SFM with the use of a cell line expressing GFP-tagged caveolin-1. This fluorescent GFP-caveolin-1 protein was found on the surface of the cells in a punctate distribution. We presume that puncta represent endogenous caveolae that had integrated the GFP-caveolin-1 fusion protein. Fluorescent spots can also be observed that are not obviously present on the surface of the cells (Friedrichson and Kurzchalia unpublished observations) but in this study, only spots that were on or very near to the surface were selected (*see* Methods). Interestingly, when the composite SFM scan of the cell surface was aligned with the green fluorescent surface caveolae spots, it was obvious that these tended to correspond to pits in the topographical SFM image (Fig. 4). Unfortunately, by aligning the fluorescent image and the SFM image it was not possible to be sure whether the caveolin spots colocalized to large or small membrane pits. In a more refined procedure, fluorescence and SFM images were captured with the same microscope, resulting in a more accurate alignment. The results from this experiment also showed that fluorescent caveolin-1 spots correlated well with pits in the SFM scan (Fig. 5). It took many attempts to obtain good-quality fluorescence and SFM images simultaneously and we could therefore not make any quantitative analysis of the results. However, this approach indicates that membrane topography imaged with the SFM technique may be directly reflected at the molecular level in the localization of endogenous caveolae. Other studies using the SFM have identified membrane pits as fusion pores by using gold-labeled antibodies against known contents of the secretory vesicle (Cho et al., 2002b). In the present study, we could not use antibodies in the same way against caveolin-1, a characteristic component of caveolae, as this protein does not have an extracellular epitope accessible from the cell surface (Anderson, 1998).

In order to provide more direct evidence that the smallest pits imaged in our experiments were indeed identical to caveolae, we took advantage of the fact that these structures are critically dependent on membrane cholesterol. At the ultrastructural level several studies have shown that after depletion of membrane cholesterol, caveolae virtually disappear from the membrane surface (Rothberg et al., 1990, 1992; Schnitzer et al., 1994; Rodal et al., 1999). Here we used methyl-β-cyclodextrin to deplete cholesterol from the plasma membrane and imaged the fixed cells directly after this procedure. Strikingly, the size distribution shifted dramatically to the right, indicating that virtually all the smallest membrane pits had disappeared from the cell membrane surface. After treatment, the size distribution was best fitted with a single normal distribution with a mean of 203 nm. It is tempting to speculate that the remaining pits represented a functionally distinct membrane organelle identical to clathrin-coated endocytic pits. Clathrin-coated pits tend to have a slightly larger open diameter in the cell membrane when visualized at the ultrastructural level (*see* for example Rodal et al., 1999). However, in this study we could provide no inde-

pendent evidence that the larger surface features do, indeed, correspond to clathrin-coated pits. Up until recently it was thought that the budding and trafficking of clathrin-coated pits was, in contrast to caveolae, independent of membrane cholesterol. However, recently two groups have reported that the budding (pinching off) of clathrin-coated pits is substantially inhibited after cholesterol depletion with methyl-β-cyclodextrin (Rodal et al., 1999; Subtil et al., 1999). Examination of the clathrin-coated pits at the ultrastructural level, however, indicated that pits were still present but were shallow compared to those observed in control cells (Subtil et al., 1999). In the same cells, caveolae were found to be absent after the same treatment (Rodal et al., 1999). The slight increase (10%) in the diameter of the middle-sized pits (from 190 nm to 203 nm) in our experiments is consistent with the observed flattening of coated pits in these recent reports (Rodal et al., 1999; Subtil et al., 1999).

Together our data indicate that it is indeed possible to image and identify membrane pits as caveolae in both living and lightly fixed cells. The great advantage offered by the SFM technique is that the surface features of the cell membrane can be examined quickly (in minutes) in three dimensions without special treatment of the cell with strong fixatives or heavy metals. In this study we have concentrated on identifying structures imaged with SFM with a known, functionally important membrane organelle, the caveolae. Previous studies have succeeded in using the SFM to image membrane pits on the surface of secretory cells, such as the pancreatic acinar cell (Schneider et al., 1997; Cho et al., 2002a). It is even possible to image the dynamics of vesicle fusion-associated secretory events (Schneider et al., 1997). In the present study, we have not attempted to look in detail at the dynamics of membrane pits on the surface of living cells, although in the course of this study, it was sometimes observed that pits disappeared periodically during scanning in living cells. The experimental demonstration here that the smallest membrane pits observed with the SFM on the surface of CHO cells are identical to caveolae, is an important step in developing the SFM technique to study the biology of caveolae in intact cells.

This work was supported by grants from the Deutsche Forschungs Gemeinschaft and the Max-Delbrück Center for Molecular Medicine. HL was supported through a grant from the European Community Social fund. Additional support was obtained from a Human Frontiers Science Program grant to TVK. We gratefully acknowledge the excellent technical assistance of Iska Liebner.

References

Anderson, R.G.W. 1998. The caveolae membrane system. *Annu. Rev. Biochem.* **67:**199–225

Brown, D.A., London, E. 1998. Functions of lipid rafts in biological membranes. *Annu. Rev. Cell. Dev. Biol.* **14:**111–136

Bustamante, C., Rivetti, C., Keller, D.J. 1997. Scanning force microscopy under aqueous solutions. *Curr. Opin. Struct. Biol.* **7:**709–716

Cho, S.J., Quinn, A.S., Stromer, M.H., Dash, S., Cho, J., Taatjes, D.J., Jena, B.P. 2002a. Structure and dynamics of the fusion pore in live cells. *Cell Biol. Int.* **26:**35–42

Cho, S.J., Jeftinija, K., Glavaski, A., Jeftinija, S., Jena, B.P., Anderson, L.L. 2002b. Structure and dynamics of the fusion pores in live GH-secreting cells revealed using atomic force microscopy. *Endocrinology* **143:**1144–1148

Drab, M., Verkade, P., Elger, M., Kasper, M., Lohn, M., Lauterbach, B., Menne, J., Lindschau, C., Mende, F., Luft, F.C., Schedl, A., Haller, H., Kurzchalia, T.V. 2001. Loss of caveolae, vascular dysfunction, and pulmonary defects in caveolin-1 gene-disrupted mice. *Science* **293:**2449–2452

Fra, A.M., Masserini, M., Palestini, P., Sonnino, S., Simons, K. 1995. A photo-reactive derivative of ganglioside GM1 specifically cross-links VIP21-caveolin on the cell surface. *FEBS Lett.* **375:**11–14

Goerge, T., Niemayer, P., Rogge, R., Ossig, R., Oberleithner, H., Schneider, S.W. 2002. Secretion pores in human endothelial cells during acute hypoxia. *J. Membrane Biol.* **187:**203–211

Keller, P., Simons, K. 1998. Cholesterol is required for surface transport of influenza virus hemagglutinin. *J. Cell Biol.* **140:** 1357–1367

Kilsdonk, E.P., Yancey, P.G., Stoudt, G.W., Bangerter, F.W., Johnson, W.J., Phillips, M.C., Rothblat, G.H. 1995. Cellular cholesterol efflux mediated by cyclodextrins. *J. Biol. Chem.* **270:** 17250–17256

Kurzchalia, T.V., Dupree, P., Monier, S. 1994. VIP-21 Caveolin, a protein of the trans-Golgi network and caveolae. *FEBS Lett.* **346:**88–91

Kurzchalia, T.V., Parton, R.G. 1999. Membrane microdomains and caveolae *Curr. Opin. Cell Biol.* **11:**424–431

Lesniewska, E., Giocondi, M.C., Vie, V., Finot, E., Goudonnet, J.P., Le-Grimellec, C. 1998. Atomic force microscopy of renal cells: limits and prospects. *Kidney Int.* **65:**42–48

Lobie, P.E., Sadir, R., Graichen, R., Mertani, H.C., Morel, G. 1999. Caveolar internalization of growth hormone. *Exp. Cell Res.* **246:**47–55

Maxfield, F.R., Mayor, S. 1997. Cell surface dynamics of GPI-anchored proteins. *Adv. Exp. Med. Biol.* **419:**355–364

Mayor, S., Rothberg, K.G., Maxfield, F.R. 1994. Sequestration of GPI-anchored proteins in caveolae triggered by crosslinking. *Science* **264:**1948–1951

Monier, S., Dietzen, D.J., Hastings, W.R., Lublin, D.M., Kurzchalia, T.V. 1996. Oligomerization of VIP21-caveolin in vitro is stabilized by long chain fatty acylation or cholesterol. *FEBS Lett.* **388:**143–149

Murata, M., Peranen, J., Schreiner, R., Wieland, F., Kurzchalia, T.V., Simons, K. 1995. VIP21/caveolin is a cholesterol-binding protein. *Proc. Natl. Acad. Sci. USA* **92:**10339–10343

Ohtani, Y., Irie, T., Uekama, K., Fukunaga, K., Pitha, J. 1989. Differential effects of alpha-, beta- and gamma-cyclodextrins on human erythrocytes. *Eur. J. Biochem.* **186:**17–22

Okamoto, T., Schlegel, A., Scherer, P.E., Lisanti, M.P. 1998. Caveolins, a family of scaffolding proteins for organizing "preassembled signaling complexes" at the plasma membrane. *J. Biol. Chem.* **273:**5419–5422

Rodal, S.K., Skretting, G., Garred, O., Vilhardt, F., van-Deurs, B., Sandvig, K. 1999. Extraction of cholesterol with methyl-beta-cyclodextrin perturbs formation of clathrin-coated endocytic vesicles. *Mol. Biol. Cell* **10:**961–974

Rothberg, K.G., Heuser, J.E., Donzell, W.C., Ying, Y.S., Glenney, J.R., Anderson., R.G.W. 1992. Caveolin, a protein component of caveolae membrane coats. *Cell* **68:**673–682

Rothberg, K.G., Ying, Y.S., Kamen, B.A., Anderson, R.G. 1990. Cholesterol controls the clustering of the glycophospholipid-anchored membrane receptor for 5-methyltetrahydrofolate. *J. Cell Biol.* **111:**2931–2938

Roy, S., Luetterforst, R., Harding, A., Apolloni, A., Etheridge, M., Stang, E., Rolls, B., Hancock, J.F., Parton, R.G. 1999. Dominant-negative caveolin inhibits H-Ras function by disrupting cholesterol-rich plasma membrane domains. *Nature Cell Biol.* **1:**98–105

Scheel, J., Srinivasan, J., Honnert, U., Henske, A., Kurzchalia, T.V. 1999. Involvement of caveolin-1 in meiotic cell-cycle progression in *Caenorhabditis elegans*. *Nature Cell Biol.* **1:**127–129

Schnitzer, J.E., Oh, P., Pinney, E., Allard, J. 1994. Filipin-sensitive caveolae-mediated transport in endothelium: reduced transcytosis, scavenger endocytosis, and capillary permeability of select macromolecules. *J. Cell Biol.* **127:**1217–1232

Schneider, S.W., Sritharan, K.C., Geibel, J.P., Oberleithner, H., Jena, B.P. 1997. Surface dynamics in living acinar cells imaged by atomic force microscopy: identification of plasma membrane structures involved in exocytosis. *Proc. Natl. Acad. Sci.* **94:**316–321

Subtil, A., Gaidarov, I., Kobylarz, K., Lampson, M.A., Keen, J.H., McGraw, T.E. 1999. Acute cholesterol depletion inhibits clathrin-coated pit budding. *Proc. Natl. Acad. Sci. USA* **96:** 6775–6780

Westermann, M., Leutbecher, H., Meyer, H.W. 1999. Membrane structure of caveolae and isolated caveolin-rich vesicles. *Histochem. Cell. Biol.* **111:**71–81

Yamada, E. 1955. The fine structure of the gall bladder epithelium of the mouse. *J. Biophys. Biochem. Cytol.* **1:**445–458